Title
METALLOGRAPHIC AND DIFFERENTIAL SCANING CALORIMETRY ANALYSES OF PRECIPITATION AND RECRYSTALLIZA-TION IN AN Al-Mn ALLOY

Author
Howe, J.M.

Publication Date
1985-07-01

LBL-19989
Preprint

Lawrence Berkeley Laboratory
UNIVERSITY OF CALIFORNIA

Materials & Molecular Research Division

To be submitted for publication

METALLOGRAPHIC AND DIFFERENTIAL SCANNING CALORIMETRY ANALYSES OF PRECIPITATION AND RECRYSTALLIZATION IN AN Al-Mn ALLOY

J.M. Howe

July 1985

Prepared for the U.S. Department of Energy under Contract DE-AC03-76SF00098

DISCLAIMER

Metallographic and Differential Scanning Calorimetry Analyses of Precipitation and Recrystallization in an Al-Mn Alloy

J.M. Howe

Materials and Molecular Research Division
Lawrence Berkeley Laboratory
Department of Materials Science and Mineral Engineering
University of California, Berkeley, CA 94720

ABSTRACT

Complimentary optical and transmission electron microscopy and differential scanning calorimetry analyses were used to study the interaction between precipitation and recrystallization in aluminum alloy 3003, thermomechanically treated to produce different initial states of strain hardening and manganese supersaturation. These studies show that precipitation of manganese on subgrain boundaries prior to recrystallization results in a coarse, elongated grain structure, which is often undesirable in commercial alloys of this type. The results also demonstrate the effectiveness of differential scanning calorimetry for analyzing microstructural problems associated with transition elements in aluminum alloys.

I. INTRODUCTION

Aluminum alloys are ideally suited for study by differential scanning calorimetry (DSC) because their good thermal conductivities and relatively low melting points permit examination of most solid/solid and solid/liquid reactions in a high-sensitivity, low-temperature (< 600°C) cell. While many

microstructural features that are analyzed by DSC can also be observed by other metallographic methods, DSC has the advantages of: 1) analyzing comparatively large volumes of material, 2) quantitative data output, and 3) minimal time and sample preparation.

To date, a number of investigators have examined the basic precipitation processes in 2000 series Al-Cu,[1-4] 5000 series Al-Mg,[5,6] 6000 series Al-Mg-Si[7-12] and 7000 series Al-Mg-Zn[13-18] alloys by DSC. These age-hardening alloys involve relatively fast-diffusing atomic species and have large enthalpies of reaction, making them well-suited for analysis by DSC. However, there have been few detailed DSC studies concerned with the precipitation of transition elements in Al alloys.[19] These elements generally require much higher temperatures for diffusion and precipitation, and it is uncertain whether the low enthalpies expected for such reactions are suitable for analysis by DSC. Since the properties of many important commercial Al alloys depend on the precipitation of such elements and in particular, on the interaction between the precipitation of transition elements and concurrent recrystallization, the following study was performed. The purpose of this study was to determine whether DSC is a suitable technique for analyzing the effects of: 1) supersaturation of transition elements, and 2) second-phase dispersition characteristics on the recovery and recrystallization behavior of wrought Al alloys. An Al-Mn alloy was chosen for this study because of the relative ease of obtaining rather large supersaturations.[20]

II. EXPERIMENTAL PROCEDURES

Spectrographic analyses of the 3003 alloy used in this study are given in Table I, together with the Aluminum Association limits for 3003 alloy. The starting material was 25.4 mm thick hot-rolled plate. Three pieces of the plate were solution annealed at 643°C for 24 hrs. Samples I and III were subsequently quenched in cold water while sample II was transferred to a furnace at 454°C and held for 24 hrs., followed by an air cool. Samples II and III were then cold-rolled about 80% to 4.9 mm thickness. Each of these thermomechanical treatments is illustrated schematically in Figures 1(a-c). These treatments produced samples with essentially three different microstructures: 1) sample I was highly supersaturated with Mn (~ 0.8%), 2) sample II was highly precipitated (~ 0.2% Mn in solution) and strain hardened, and 3) sample III was highly supersaturated strain hardened. [20-23]

DSC specimens were cut from each of the three samples and ground to 650 mg weight on a SiC water wheel. A similar mass of annealed 99.99% Al was used as a reference. The DSC analyses were performed on a DuPont 900 Thermal Analyzer equipped with a DSC cell. DSC thermograms were obtained from each of the three samples at heating rates of 2, 5 and 20°C/min. A heating rate of 2°C/min is considered to be relatively fast when compared with a commercial coil anneal, which may average only about 0.6°C/min. In addition, the following experiment was performed in order to characterize each peak in the DSC thermo-

grams. Several 31.8 mm squares were cut from samples I-III and heated in a large furnace at precisely 5 °C/min to simulate the DSC analyses at the same heating rate. These were subsequently quenched in cold water at temperatures of interest, as determined from the DSC thermograms. Rockwell hardnesses and %IACS conductivities were determined on the starting samples and on each of the quenched samples. These are given in Table II, where the exact quenching temperatures are also indicated.

The precipitate and grain structures of all the samples were examined by optical metallography and where necessary, by transmission electron microscopy (TEM). The grain structures of the samples were examined at 100X magnification using a sulphuric acid anodize and polarized light. The Mn dispersion was then revealed by removing the anodized coating in a hot phosphoric acid solution and examining at 250X magnification. TEM specimens were prepared by jet-polishing in a 25% nitric acid/75% methanol electrolyte at 10-12 V and -20 °C. Thin foils were examined in bright-field at 10-40kX magnification in a JEOL 100CX microscope operating at 100 keV. In addition, precipitate and grain structures were compared among the DSC samples after heating to 600 °C at the three different rates. A few of these samples were also examined in the scanning electron microscope (SEM) at 1 and 10kX, for comparison with optical metallography. The SEM specimens were relief-etched in a 2.5% solution of potassium iodide in methanol for 30 sec at 30 V.[4] They were examined in an ISI Super IIIA SEM at 30 keV using secondary electron imaging and a 30° tilt.

III. RESULTS AND DISCUSSION

A. Sample I.

The 5°C/min DSC thermogram for sample I is shown in Figure 2, together with graphs of the conductivity and hardness versus quenching temperature. The grain structure and Mn dispersion of the starting sample (25°C) are also shown in Figures 3(a) and (b). Notice the large recrystallized grains in Figure 3(a), and the clear areas in Figure 3(b) in between the coarse intermetallic particles remaining from the casting and rolling procedures.[20,22] As the sample is heated from 25 to 600°C, one major reaction is evident, a large exothermic reaction with a maximum at about 468°C. Figure 3(c) shows that the microstructure is almost entirely black at this temperature due to a very fine, dense Mn dispersion. This maximum thus represents the maximum rate of Mn precipitation. An increase of 2.4 %IACS conductivity and a negligible decrease in hardness accompany the reaction, as illustrated in Figure 2. After further heating to 600°C, the precipitates have coarsened and individual particles are evident, as shown in Figure 3(d). The background has also become clearer due to dissolution and/or coalescense of the precipitates. A slight drop in conductivity also occurs between 468 and 600°C (Figure 2), further indicating that some dissolution of Mn is occurring. A small decrease in hardness also occurs, lending further evidence that the precipitates are coarsening, and that the interparticle spacing is increasing.[24,25]

Notice that all of these reactions are apparent in the DSC thermogram in Figure 2, demonstrating that DSC can be used to follow the precipitation of Mn in Al. There are also subtle exothermic changes in the DSC thermogram between 100 to 200°C, and at about 400°C. These exotherms may be due to effects such as precipitation of metastable phases or phases of different composition, i.e. αAl(Fe,Mn)Si and (Fe,Mn)Al$_6$ are both known to precipitate in this system.[20] However, no attempt was made to identify the exact types of precipitates in this study. It should also be noted that the grain structure of this sample did not appear to change appreciably after heating to 600°C.

The DSC thermograms for sample I at all three heating rates are shown in Figure 4(a), and the start, maximum rate and finish of precipitation are plotted as a function of heating rate in Figure 4(b). Only two reactions are evident in Figure 4(a) for the 5 and 20°C/min samples: 1) precipitation of Mn between about 325 and 550°C, and 2) slight dissolution of Mn above about 550°C. This is assuming that dissolution of Mn above 550°C is precluding any exothermic reaction accompanying coarsening of the Mn precipitates. Since the DSC thermogram of the 2°C/min sample rises above 550°C, it may indicate that coarsening of the Mn dispersoids is favored over dissolution at this heating rate. This was not verified experimentally, however. Also notice from Figure 4(b) that the reaction temperatures do not increase linearly with heating rate but rather, level off at higher heating rates. This effect indicates that

the precipitation of Mn is limited kinetically at the higher heating rates, i.e. that the precipitation of Mn is a relatively slow process, which kinetically lags behind the 20°C/min heating rate employed.[26-28]

B. Sample II.

The 5°C/min DSC thermogram for sample II is shown in Figure 5, again with graphs of the conductivity and hardness versus quenching temperature. Optical and TEM micrographs at each stage in the DSC thermogram are shown in Figures 6 through 8. Notice that the grain structure of the starting material in Figure 6(a) is heavily worked, consisting mainly of long, rectangular dislocation cells and tangles, as shown in Figure 6(c). This material also has a relatively clear background when etched to reveal the Mn dispersoids, because most of the Mn has been precipitated out of solution in the form of coarse particles (Figure 6(b)).

As the sample is heated from 25°C, a rather low, broad peak occurs in the DSC thermogram between about 275 and 310°C. Figure 6(d) shows that at 290°C, which is near the center of this peak, the optical grain structure is indistinguishable from that of the starting material, although further precipitation of Mn has occurred by this temperature, as evident from Figure 6(e). However, TEM reveals that recovery has progressed to a large extent in some areas of the sample at 290°C, as illustrated by the polygonized subgrains in Figure 6(f). Thus, the low, broad peak between about 275 and 310°C is mainly due to

recovery. These precipitation and recovery processes produce a slight change in conductivity (~ 0.6 %IACS) and a small change in hardness (~ 2.4 R_H) in the sample.

As sample II is further heated, a sharp peak occurs at 333 °C, immediately following the low, broad peak associated with recovery. The relative shapes and positions of these two peaks are very similar to the power difference which occurs for recovery and recrystallization in 99.99% Al deformed 75% in compression, as shown by Clareborough et al.[29] Figure 7(a) shows the grain structure at 333 °C. The sample was largely recrystallized near the surface, but the amount of recrystallization diminished toward the center, which is shown in Figure 7(a). The recrystallized grains are relatively equiaxed. The TEM micrograph in Figure 7(c) shows an interface between two recrystallized grains and many subgrains, typical of partially recrystallized areas. Many micron-sized Mn precipitates from the annealing treatment are distributed throughout a portion of the micrograph, but also notice the fine precipitates indicated by arrows in the top-right corner. The arrangement of these precipitates indicates that they formed on the original dislocation cells and subgrains, and were left behind as the recrystallized grains passed through.[30] This observation agrees with the optical micrograph in Figure 6(e), which showed that some precipitation had occurred either before or concurrent with recovery. The relatively equiaxed grain structure which developed in this sample, however, indicates that these precipitates did not exert a large grain boundary pinning effect.[31-35]

Further precipitation also occurred between 290 and 333°C, as is evident by comparing Figure 7(b) with Figure 6(e), but the amount is relatively small. Thus, the peak at 333°C represents recrystallization and the start and finish of recrystallization can be determined from the temperatures on either side of the base of this peak.[28] Several recrystallized grains were also observed to be nucleating from the intermetallic particles (arrow in Figure 7(d)), indicating that these large particles contribute towards nucleation and a fine grain size.[30,31,35,36] The particle shown in Figure 7(d) is about 1.5 μm wide. A slight increase in conductivity (~ 0.7 %IACS) and a large decrease in hardness (25.8 R_H) accompanied the slight precipitation and partial recrystallization at 333°C.

Optical and TEM structures for this sample after heating to 470 and 600°C are shown in Figure 8. By 470°C recrystallization is complete (Figure 8(a)), and although it is not apparent by comparing the optical micrographs in Figures 7(b) and 8(b), the fine subgrain precipitates which were just visible in Figure 7(c) have grown to the extent that they are now clearly visible, as indicated by the arrows in the TEM micrograph in Figure 8(c). These changes produce a steady rise in the DSC thermogram between about 360 and 470°C, and are accompanied by a slight increase in conductivity (~ 0.6 %IACS) and a further reduction in hardness (~ 14.4 R_H). By 600°C, slight grain growth has occurred (compare Figure 8(d) with 8(a)) and most of the Mn which precipitated at the lower temperatures has dissolved, as indicated by the clear background in Figure 8(e). These changes produce a steady decrease in the DSC thermogram and are accom-

panied by a decrease in conductivity of 1.8 %IACS, and virtually no change in hardness.

The DSC thermograms for sample II at all three heating rates are shown in Figure 9(a), and the start of recovery, maximum rate of recrystallization and maximum rate of high-temperature precipitation are plotted versus heating rate in Figure 9(b). As with sample I, the DSC thermogram at 2°C/min rises above about 500°C, indicating that coarsening of the Mn dispersoids may be favored over dissolution at this heating rate while at 20°C/min, the thermogram steadily decreases above about 480°C, indicating that dissolution of Mn is occuring. The 5°C/min thermogram appears to lie between these two extremes. This effect causes the maximum rate of precipitation to appear to decrease with increasing heating rate in Figure 9(b), which is the reverse of the situation for the highly supersaturated sample in Figure 4(b). Also notice from Figure 9(b), that the start of recovery and particularly, the maximum rate of recrystallization, increase almost linearly with heating rate, indicating that they are not limited kinetically at the faster heating rates,[26,27] which is again opposite of the behavior for the precipitation of Mn in sample I in Figure 4(b). Also notice that the low, broad peak associated with recovery decreases in both height and width as the heating rate is increased. In fact, it is barely present in the 20°C/min DSC thermogram, indicating that recrystallization occurs almost spontaneously, without a recovery period. Also notice that a broad exothermic reaction

occurs in the 2 and 5°C/min DSC thermograms between about 100 to 250°C. These reactions are probably associated with the slight precipitation of Mn on the initial dislocation structure; however, no TEM samples were examined in this temperature range.

C. Sample III.

The 5°C/min DSC thermogram for sample III is shown in Figure 10, also with graphs of the conductivity and hardness versus quenching temperature. The grain structure and Mn dispersion of the starting sample (25°C) are shown in Figures 11(a)-(c). The sample is largely void of fine Mn precipitates and contains long subgrains filled with dislocation tangles, similar to sample II. As this sample is heated to 291°C, a low, broad peak occurs between about 100 to 200°C. As for the previous samples, this peak is thought to be due to slight precipitation of Mn on the dislocation structure and possibly, some minor rearrangement of dislocations, although no samples were observed from this region. At 291°C, a small but sharp peak occurs in the DSC thermogram. No changes are apparent in the optical grain structure at this temperature (compare Figures 11(d) and 11(a)); however, Figure 11(e) shows that a significant quantity of Mn has precipitated from solution. In particular, notice how the Mn precipitates outline the shear bands (arrows in Figure 11(e)) indicating that they have precipitated on the pre-existing dislocation structure. The TEM micrograph in Figure 11(f) shows that the long, rectangular dislocation substruc-

ture still remains at 291°C, although some recovery has occurred. In this micrograph, the Mn precipitates are very fine and difficult to distinguish from the dislocations in the subgrain boundaries. Thus, it is possible to conclude from this information that the small peak at 291°C in Figure 10 is due to the rapid precipitation of Mn on the initial dislocation structure. This precipitation causes a 0.9 %IACS decrease in conductivity and essentially no change in hardness.

As the sample is further heated, a broad exothermic reaction starts at about 310°C, causing the DSC thermogram to rise rapidly until about 340°C, and then level off until about 380 °C. Although the optical grain structure appeared unchanged at 360°C (near the center of the broad peak), TEM images at this temperature (Figure 12(b)) show that the long, rectangular subgrains are starting to polygonize and that recovery is occurring, similar to the processes observed for sample II at 290°C. In addition, a dense dispersion of Mn has precipitated throughout the matrix (Figure 12(a)) and the Mn precipitates on the subgrain boundaries have coarsened to the extent that they are clearly visible, as indicated by the arrows in Figure 12(b). Although it is difficult to see in Fig. 12(b), the fine matrix precipitates were visible at higher magnifications. Thus, as for sample II, the broad character of the peak between 310 and 380°C is due to recovery processes, although the exothermic effects associated with these processes are superimposed on a much larger exothermic reaction which is due to the precipita-

tion of a large amount of Mn. A 2.2 %IACS increase in conductivity occurs from 291 to 360°C due to the abundant precipitation of Mn and the hardness decreases by about 3.5 R_H, mostly due to recovery.

Further heating of this sample produces a sharp peak at 398°C, immediately following the broad exothermic reaction due to recovery and precipitation of Mn. The shape and magnitude of this peak are similar to the peak associated with recrystallization in sample II. The optical grain structure in Figure 13(a) shows that recrystallization has started and unlike the previous sample II, the recrystallized grains in this sample have large aspect ratios, rather than being nearly equiaxed. In addition, this sample was about 50% recrystallized evenly across its thickness. Although the Mn precipitates in the optical micrograph in Figure 13(b) do not look very different from 360°C, they are now visible throughout the matrix and at the subgrain boundaries, as shown by the TEM micrographs in Figures 13(c) and (d). Figure 13(c) shows a boundary between a recrystallized grain and a number of subgrains. The arrangement of the Mn precipitates within the recrystallized grain is clearly an effect of prior precipitation on the initial dislocation structure.[30] Figure 13(d) shows the precipitates along several subgrain boundaries and in the matrix. As demonstrated by this figure, the precipitates are effectively pinning the subgrain boundaries with the result that the recrystallized grains are highly elongated, because grain growth is easier than the

nucleation of new grains.[30-33] The reactions at 398°C were accompanied by a further increase in conductivity (~ 2.6 %IACS) and a decrease in hardness of 14.9 R_H.

Subsequent heating above 398°C produces changes similar to those in sample II. At 480°C recrystallization is complete, and the elongated shape of the recrystallized grains is now clearly apparent (Figure 14(a)). Although further precipitation of Mn and precipitate coarsening are revealed by the TEM micrograph in Figure 14(c), only a slight change in the Mn dispersion is apparent optically (compare Figures 14(b) and 13(b)). These changes caused a 1.7 %IACS increase in conductivity and a decrease in hardness of 17.1 R_H. Heating to 600°C results in slight grain growth (Figure 14(d)) and possibly, some precipitate coalescense (compare Figures 14(b) and 14(e)), but these effects are predominated by the dissolution of Mn between about 450 and 600°C. A substantial amount of Mn has dissolved by 600 °C, as evidenced by a decrease in the conductivity of 5.5 %IACS. Grain growth also produces a further drop in hardness of 4.2 R_H.

The DSC thermograms for sample III at heating rates of 2, 5 and 20°C/min are shown in Figure 15(a), and the start of precipitation, the start of recovery, the maximum rate of recrystallization and the end of precipitation are plotted as a function of the heating rate in Figure 15(b). Notice that unlike the previous samples, the DSC thermograms for sample III in Figure 15(a) all display endothermic reactions above about 480°C, indicating that dissolution of Mn is favored over coarsening in this sample. This is probably because the major-

ity of Mn precipitates are finer in sample III and thus, dissolve rather than coarsen at the higher temperatures, even when the heating rate is only 2°C/min. The fineness of these precipitates is most likely due to the fact that the rapid precipitation of Mn on the initial dislocation structure establishes a very dense distribution of fine precipitates. Also notice that in Figure 15(b) the low, broad peak associated with recovery decreases in width as the heating rate is increased, displaying the same behavior as the recovery peak in sample II. However, this peak is still significant at the 20°C/min heating rate. In addition, the maximum rate of recrystallization increases nearly linearly with the heating rate, again indicating that this process is not as kinetically limited as the precipitaton of Mn.

D. Comparison of Samples I-III at the 5°C/min Heating Rate.

Several interesting features are apparent when the 5°C/min DSC thermograms, conductivities and hardnesses for samples I, II and III are compared side-by-side, as shown in Figures 16(a) and (b). First, notice from Figure 16(a), that the maximum rate of high-temperature Mn precipitation occurs at about 470°C for both sample I, which is annealed and has a high supersaturation of Mn, and sample II, which is strain hardened but has a low Mn supersaturation. However, in sample III, which possesses both a high Mn supersaturation and an initial strain hardened condition, the maximum rate of precipitation occurs at a much lower

temperature of about 360°C, because the Mn solid solution is highly unstable in the presence of the initial dislocation structure.[33,34] This effect is also reflected in the graphs of the conductivities for these three samples, shown in Figure 16(b). Notice that the maximum conductivity attained in sample III is much greater than in sample II, due the to presence of the dislocation structure, and even slightly greater than the highest conductivity attained by sample II, which received an initial annealing treatment. The effect of this annealing treatment is clearly apparent by comparing the conductivities among samples I-III at 25°C in Figure 6(b). Also notice that the maximum conductivity of all of the samples occurs at about 470°C, before dissolution of Mn starts at higher temperatures.

Another feature apparent from Figures 16(a) and (b) is that both recovery and recrystallization start at much lower temperatures in sample II, where there is only a small amount of Mn in solution than in sample III, which is highly supersaturated with Mn. This observation agrees with the results of previous investigators[31-33] and can also be seen by comparing the temperatures associated with these processes in Figures 9(b) and 15(b). Also notice that the hardnesses of samples II and III in Figure 16(b) are nearly the same at 25°C due to their initial strain hardened conditions, but that the hardness of sample II decreases more readily than that of sample III at temperatures greater than about 300°C. This is clearly due to the high supersaturation of Mn, which pins the dislocation

structure and retards recrystallization in sample III, and also to the fewer number of larger (> 1 μm) particles which act as nuclei for recrystallization (Figure 7(d)).

E. Effect of Heating Rate on Grain Structure and Precipitate Dispersion.

Figures 17(a)-(c) show the grain structures which resulted in samples I-III after heating to 600°C at 2, 5 and 20°C/min in the DSC cell. Except for slight variations, the recrystallized grain structures were essentially the same, regardless of the heating rate employed. Thus, the heating rate did not affect the final grain structure over the range examined. The difference between the fine, equiaxed grains in sample II the larger, elongated grains in sample III and are clear in these micrographs.

Figures 18(a)-(c) show a similar series of micrographs revealing the precipitate distributions in each of the samples after heating to 600°C at the three different heating rates. In this case, the different heating rates do appear to have produced slightly different precipitate dispersions in samples I and III. Notice the precipitate-free zones along the grain boundaries in these samples at the 2 and 5°C/min heating rates which are not present at 20°C/min. In addition, the severity of the precipitate-free zones appears to steadily decrease with increasing heating rate, as seen by comparing the three microstructures in Figure 18(a). Also notice the difference between

the final distribution of the Mn precipitates in sample II, which received an annealing treatment, and samples I and III, which had a high initial Mn supersaturation.

Lastly, Figures 19(a)-(c) show relief-etched SEM micrographs of the large Mn particles and fine dispersoids in each of the samples after heating to 600°C at 5°C/min. When compared with the 5°C/min samples in Figures 18(a)-(c), this series of micrographs demonstrates that in general, dense distributions of fine Mn precipitates produce darker backgrounds in the optical micrographs. This can be seen by noting that sample I in Figure 18(a) displays the darkest contrast, followed by samples III and II in Figures 18(c) and 18(b), respectively. In the SEM micrographs in Figure 19, sample I contains the finest precipitates, followed by samples III and II, in that order, as evident by comparing the small Mn dispersoids indicated by arrows in the series of higher-magnification micrographs. This same feature was also indicated by several of the pevious optical and TEM micrographs. However, also note that the total volume fraction of fine Mn dispersoids in sample I (Figure 19(a)) is slightly less than that of samples II and III in Figures 19(b) and 19(c), as seen by comparing the conductivities of these samples at 600°C in Figure 16(b).

IV. CONCLUSIONS

This study was performed in order to determine whether DSC can be used to analyze the effects of: 1) supersaturation of transition elements, and 2) second-phase dispersion characteristics on the recovery and recrystallization behavior of wrought Al alloys. An Al-Mn alloy was investigated because it is possible to obtain significant Mn supersaturations and also, because this is a commercially important system which is relatively well-understood. The results of this study demonstrate that:

1. DSC is sensitive to both the precipitation and dissolution of Mn in 3003 alloy, thus demonstrating that it is a suitable technique for studing the behavior of transition elements in Al alloys.
2. DSC can be used to follow recovery and recrystallization in this alloy, and to determine the effects of concurrent precipitation of Mn on these processes.
3. Precipitation of Mn on subgrain boundaries prior to recrystallization results in the coarse, elongated grain structure which is undesirable in commercial alloys of this type.

ACKNOWLEDGEMENTS

The is author is grateful to D.D. Przybycien for running the DSC experiments, to G.W. Franti and N.Y.C. Yang for performing the TEM analyses, to W.R. Mohondro and T.D. Gibson for performing the heat treatments, to S.G. Roberts for suggesting

this project and to Kaiser Aluminum and Chemical Corporation for permission to publish the results. This study was performed in 1981, while the author was employed at the Kaiser Center for Technology. The author is also grateful to R. Gronsky of the Lawrence Berkeley Laboratory for support by the Director, Office of Energy Research, Office of Basic Energy Sciences, Materials Science Division of the U.S. Department of Energy under contract No. DE-AC03-76SF00098.

REFERENCES

1. D.S. Thompson: Thermal Analysis, Academic Press, New York, NY, 1969, vol. 2, pp. 1147-70.
2. K. Hiraon and H. Iwasaki: Trans. Japan Inst. Metals, 1964, vol. 5, pp. 162-170.
3. J.M. Papazian: Metall. Trans. A, 1981, vol. 12A, pp. 269-79.
4. J.M. Howe: Metallography, 1983, vol. 16, pp. 275-86.
5. R. Nozato and S. Ishihara: Trans. Japan Inst. Metals, 1980, vol. 21(3), pp. 580-85.
6. K. Osamura and T. Ogura: Metall. Trans. A, 1984, vol. 15A, pp. 835-42.
7. H. Sizuki, M. Hanno, Y. Shiraishi and K. Hanawa: J. Japan Inst. Light Metals, 1979, vol. 29(12), pp. 575-81.
8. J. Hajdu, L. Kertesz, Cs. Lenart and E. Nagy: Cryst. Lattice Defects, 1974, vol. 5, pp. 177-80.
9. L. Kertesz, Cs. Lenart and M. Kovacs-Treer: Cryst. Lattice Defects, 1977, vol. 7, pp. 177-80.

10. L. Kertesz, Cs. Lenart and M. Kovacs-Treer: Cryst. Lattice Defects, 1979, vol. 8, pp. 99-104.

11. L. Kertesz, M. Kovacs-Treer and J. Kollar: Cryst. Lattice Defects, 1979, vol. 8, pp. 149-52.

12. C. Garcia Cordovilla and E. Louis: Scripta Met., 1984, vol. 18, pp. 291-94.

13. K. Asano and K. Hirano: Trans. Japan Inst. Metals, 1968, vol. 9, pp. 24-34.

14. W. Lacon, H.P. Degischer, A.N. Zahra and C.Y. Zahra: Scripta Met., 1980, vol. 14, pp. 253-54.

15. R.J. DeIasi and P.N. Adler: Metall. Trans. A, 1977, vol. 8A, 1177-83.

16. P.N. Adler and R.J. DeIasi: Metall. Trans A, 1977, vol. 8A, pp. 1185-90.

17. J.M. Papazian: Mater. Sci. and Eng., 1981, vol. 51, pp. 223-30.

18. J.M. Papazian, R.J. DeIasi and P.N. Adler: Metall. Trans. A, 1980, vol. 11A, pp. 135-40.

19. P. Furrer: in Proc. 1st Riso Inter. Symp. on Metall. and Mater. Sci., 1980, pp. 109-14.

20. L.F. Mondolfo: Aluminum Alloys - Structure and Properties, Butterworths, London, 1976, pp. 324-29, 834-40, 661-63.

21. G. Marchand: Can. J. Tech., 1952, vol. 31, pp. 15-28.

22. P.R. Sperry: Trans. ASM, 1957, vol. 50, pp. 589-616.

23. E. Nes and J.D. Embury: Z. Metallkde, 1975, vol. 66, pp. 589-93.

24. A. Kelly and R.B. Nicholson: Prog. in Mater. Sci. Vol. 10 - Precipitation Hardening, Pergamon Press, Oxford, 1963, pp. 336-40.

25. E. Hornbogen and U. Koster: in Recrystallization of Metallic Materials, 2nd Edition, F. Haessner, ed., Riederer, Stuttgart, 1978, pp. 159-94.

26. M.E. Brown and C.A.R. Phillpotts: J. Chem. Education, 1978, vol. 55, pp. 556-60.

27. J.M. Papazian: Metall. Trans. A, 1982, vol. 13A, pp. 761-69.

28. W.H. Hildebrandt: Metall. Trans. A, 1979, vol. 10A, pp. 1045-48.

29. L.M. Clarebrough, M.E. Hargreaves and M.H. Loretto: Recovery and Recrystallization of Metals, Interscience Pub., New York, 1963, pp. 63-130.

30. D.J. Lloyd: Metal Sci., 1982, vol. 16, pp. 304-08.

31. E. Nes: Acta Met., 1976, vol. 24, pp. 391-98.

32. E. Nes: Aluminum, 1979, vol. 52(9), pp. 319-24.

33. G. Hausch, P. Furrer and H. Warlimont: Z. Metallkde.,1978, vol. 69, pp. 174-80.

34. P. Furrer and G. Hausch: Metal Sci., 1979, vol. 13, pp. 155-62.

35. P.R. Mould and P. Cotterill, J. Mater. Sci., 1967, vol. 2, pp. 241-255.

36. F.J. Humphreys: Metal Sci., 1979, vol. 13, pp. 136-45.

TABLES

Table I. Chemical Compositions of 3003 Alloy Investigated

	Composition (Wt Pct)							
	Si	Fe	Cu	Mn	Mg	Cr	Zn	Ti
This Study	0.24	0.63	0.15	1.07	0.004	0.001	0.030	0.020
AA Limits	0.6	0.7	0.05 0.20	1.0 1.5	-	-	0.10	-

Table II. Properties of 3003 Samples at Indicated Quenching Temperatures

Sample	Quenching Temp. (°C)	Hardness (R_H)	Conductivity (% IACS)
I	25	59.9	35.0
	468	59.4	37.4
	600	56.4	36.9
II	25	95.8	39.5
	290	93.6	40.1
	333	67.8	40.8
	470	53.2	41.4
	600	53.7	39.2
III	25	99.3	34.8
	291	98.8	35.7
	360	95.6	38.9
	398	80.7	41.5
	480	63.6	43.2
	600	58.4	37.7

FIGURE CAPTIONS

Fig. 1 - Schematic illustrations of thermomechanical treatments applied to 3003 alloy samples: (a) sample I - supersaturated and recrystallized, (b) sample II - precipitated and strain hardened, and (c) sample III - supersaturated and strain hardened.

Fig. 2 - The DSC thermogram, conductivities and hardnesses of sample I after heating to 600°C at 5°C/min. The open circles on the DSC thermogram indicate where samples were quenched for the property measurements and metallographic examination.

Fig. 3 - The grain structure and Mn dispersion in sample I: (a,b) the starting material, (c) after heating to 468°C, and (d) after heating to 600°C at 5°C/min.

Fig. 4 - (a) The DSC thermograms for sample I at heating rates of 2,5 and 20°C/min, and (b) graphs of the corresponding temperatures for the start, maximum rate and finish of precipitation as a function of heating rate.

Fig. 5 - The DSC thermogram, conductivities and hardnesses of sample II after heating to 600°C at 5°C/min. The open circles on the DSC thermogram indicate where samples were quenched for the property measurements and metallographic examination.

Fig. 6 - The grain structures and Mn dispersion in sample II: (a-c) the starting material, and (d-f) after heating to 290°C at 5°C/min.

Fig. 7 - The grain structure and Mn precipitates in sample II after heating to 333°C at 5°C/min.

Fig. 8 - The grain structures and Mn precipitates in sample II: (a-c) after heating to 470°C, and (d,e) after heating to 600°C at 5°C/min.

Fig. 9 - (a) The DSC thermograms for sample II at heating rates of 2, 5 and 20°C/min, and (b) graphs of the corresponding temperatures for the start of recovery, maximum rate of recrystallization and the maximum rate of precipitation as a function of heating rate.

Fig. 10 - The DSC thermogram, conductivities and hardnesses of sample III after heating to 600°C at 5°C/min. The open circles on the DSC thermogram indicate where samples were quenched for the property measurements and metallographic examination.

Fig. 11 - The grain structures and Mn dispersoids in sample III: (a-c) the starting material, and (d-f) after heating to 291°C at 5°C/min.

Fig. 12 - (a,b) The grain structure and Mn dispersoids in sample III after heating to 360°C at 5°C/min.

Fig. 13 - (a-d) The grain structure and Mn precipitates in sample III after heating to 398°C at 5°C/min.

Fig. 14 - (a-c) The grain structures and Mn dispersoids in sample III after heating to 480°C, and (d,e) after heating to 600°C at 5°C/min.

Fig. 15 - (a) The DSC thermograms for sample III after heating to 600°C at 2, 5 and 20°C/min, and (b) graphs of the corresponding temperatures for the start of precipitation and recovery, the maximum rate of recrystallization and the end of precipitation as a function of heating rate.

Fig. 16 - (a) The DSC thermograms for samples I-III at 5°C/min, and (b) graphs of the conductivities and hardnesses of these samples from 25 to 600°C.

Fig. 17 - The grain structures in samples I-III after heating to 600°C at 2, 5 and 20°C/min: (a) sample I, (b) sample II, and (c) sample III.

Fig. 18 - The Mn precipitates in samples I-III after heating to 600°C at 2, 5 and 20°C/min: (a) sample I, (b) sample II, and (c) sample III.

Fig. 19 - Relief-etched SEM micrographs showing the large intermetallic particles (left column) and fine Mn dispersoids (right column) in samples I-III after heating to 600°C at 5°C/min: (a) sample I, (b) sample II, and (c) sample III.

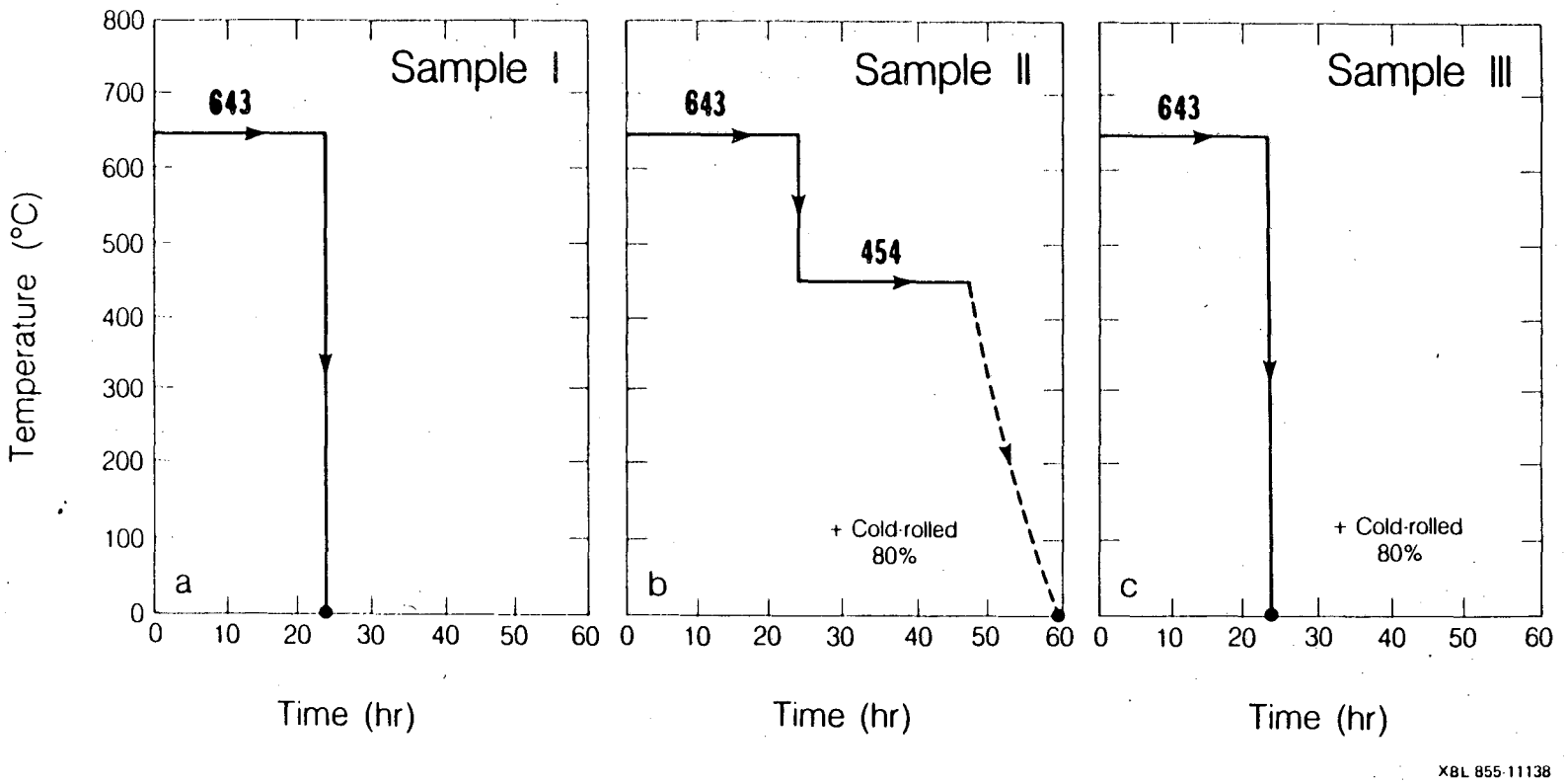
Temperature (°C)
800
700
600
500
400
300
200
100
0
Sample I
643
a
Sample II
643
454
+ Cold-rolled
80%
b
Sample III
643
+ Cold-rolled
80%
c
0 10 20 30 40 50 60
Time (hr)
XBL 855-11138

Fig. 1

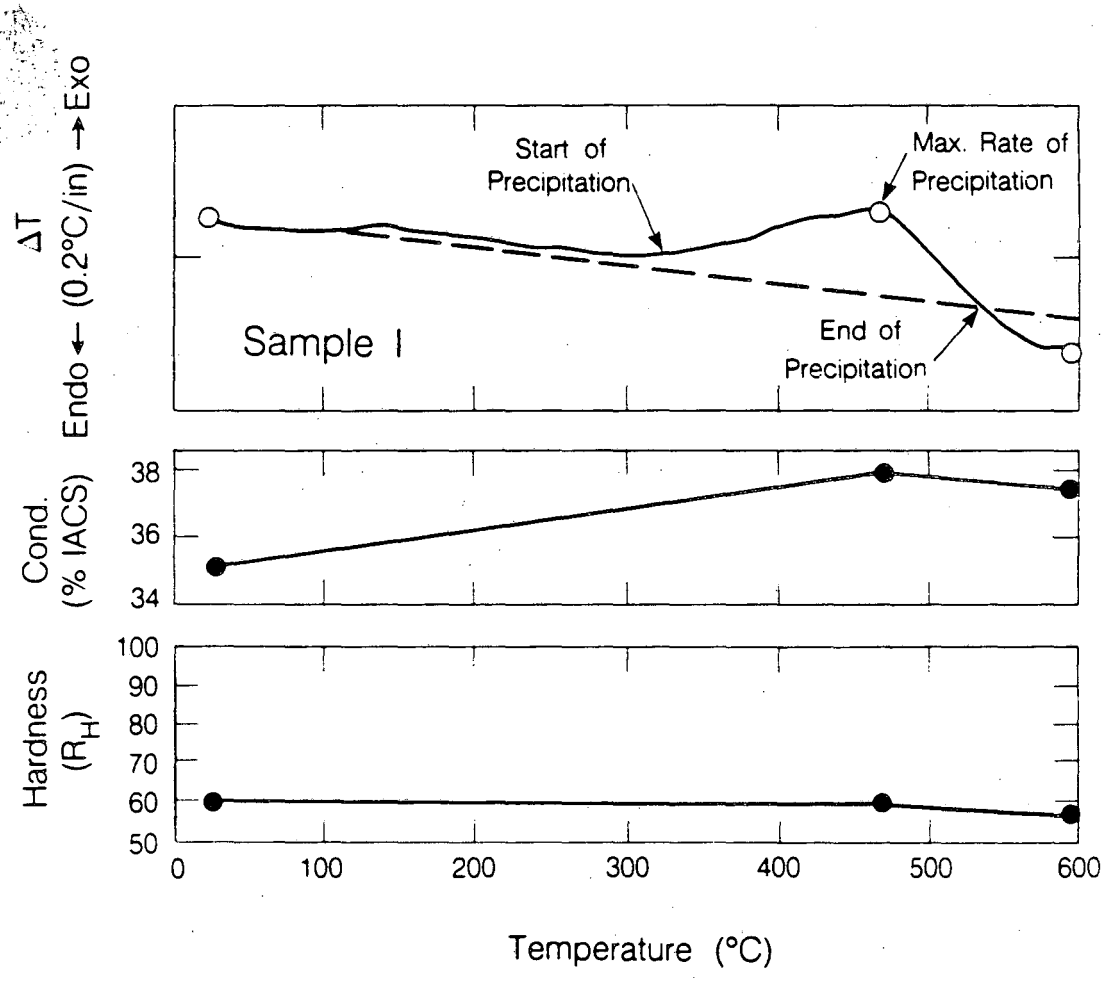
ΔT
Endo ← (0.2°C/in) → Exo
Start of Precipitation
Max. Rate of Precipitation
Sample I
End of Precipitation
Cond. (% IACS)
38
36
34
Hardness (R_H)
100
90
80
70
60
50
0
100
200
300
400
500
600
Temperature (°C)
XBL 855-11141

Fig. 2

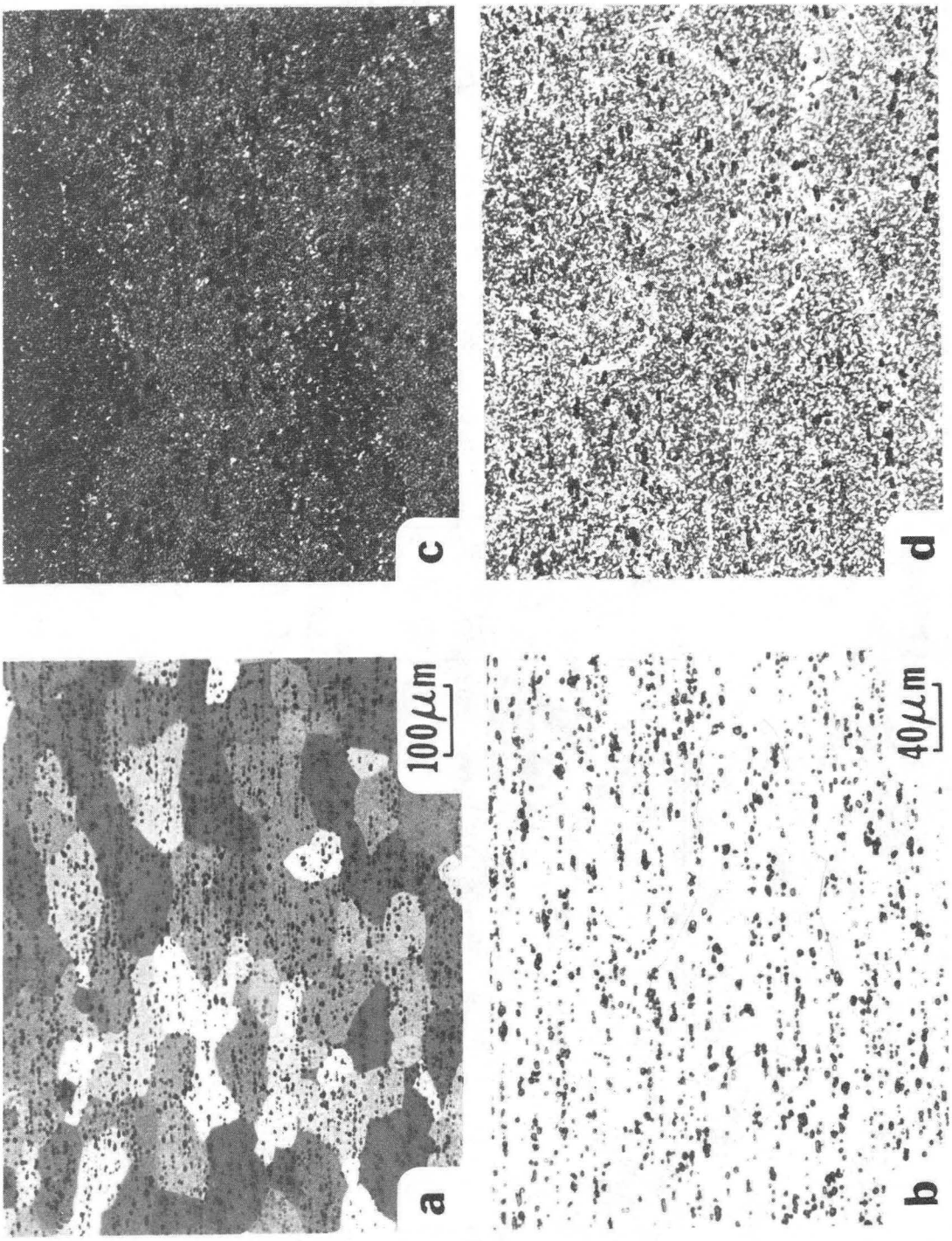

XBB 855-3947

Fig. 3

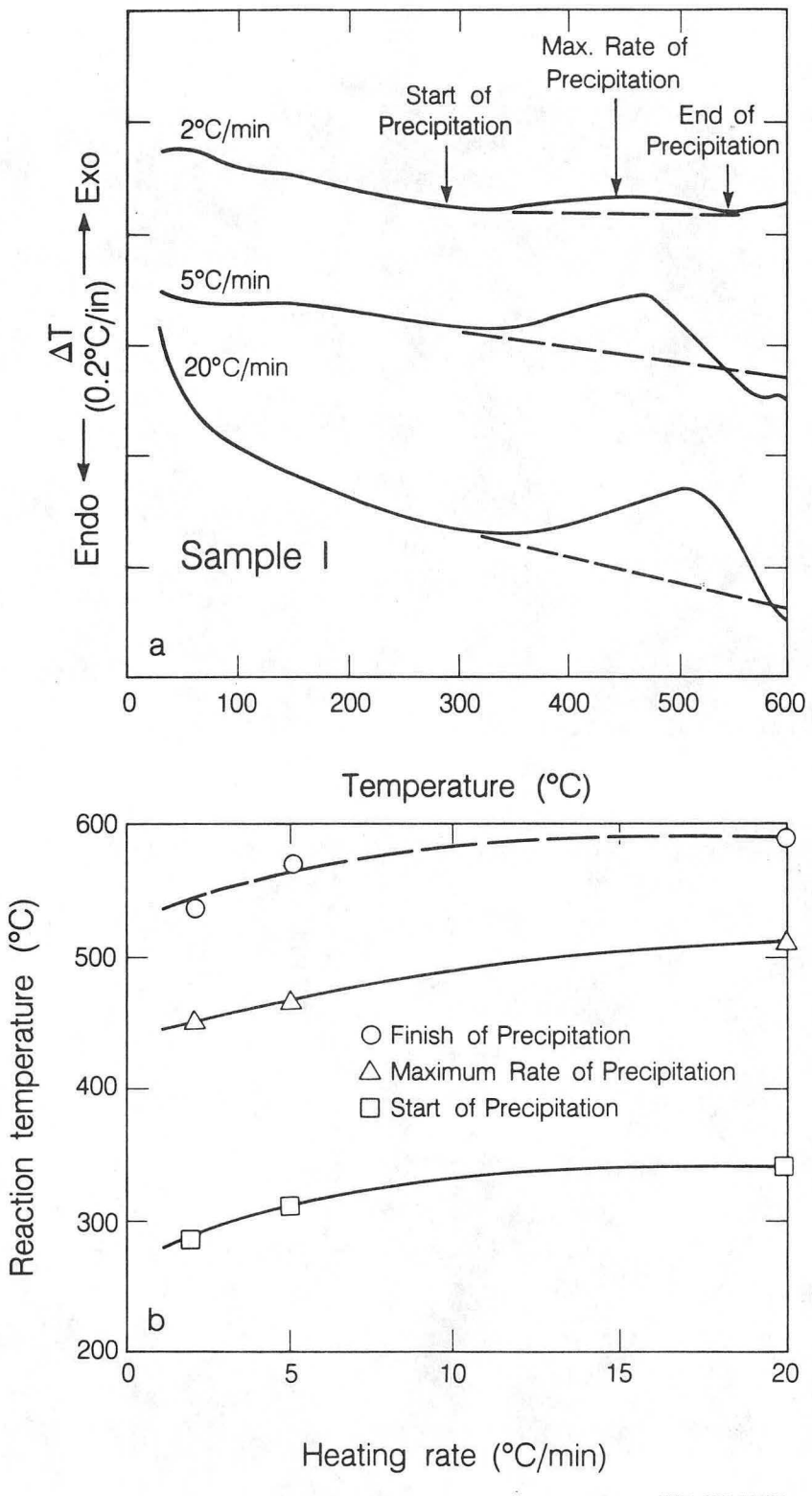
Max. Rate of Precipitation
Start of Precipitation
End of Precipitation
2°C/min
5°C/min
20°C/min
Sample I
a
ΔT (0.2°C/in)
Endo
Exo
0
100
200
300
400
500
600
Temperature (°C)
Reaction temperature (°C)
600
500
400
300
200
Finish of Precipitation
Maximum Rate of Precipitation
Start of Precipitation
b
0
5
10
15
20
Heating rate (°C/min)
XBL 855-11129

Fig. 4

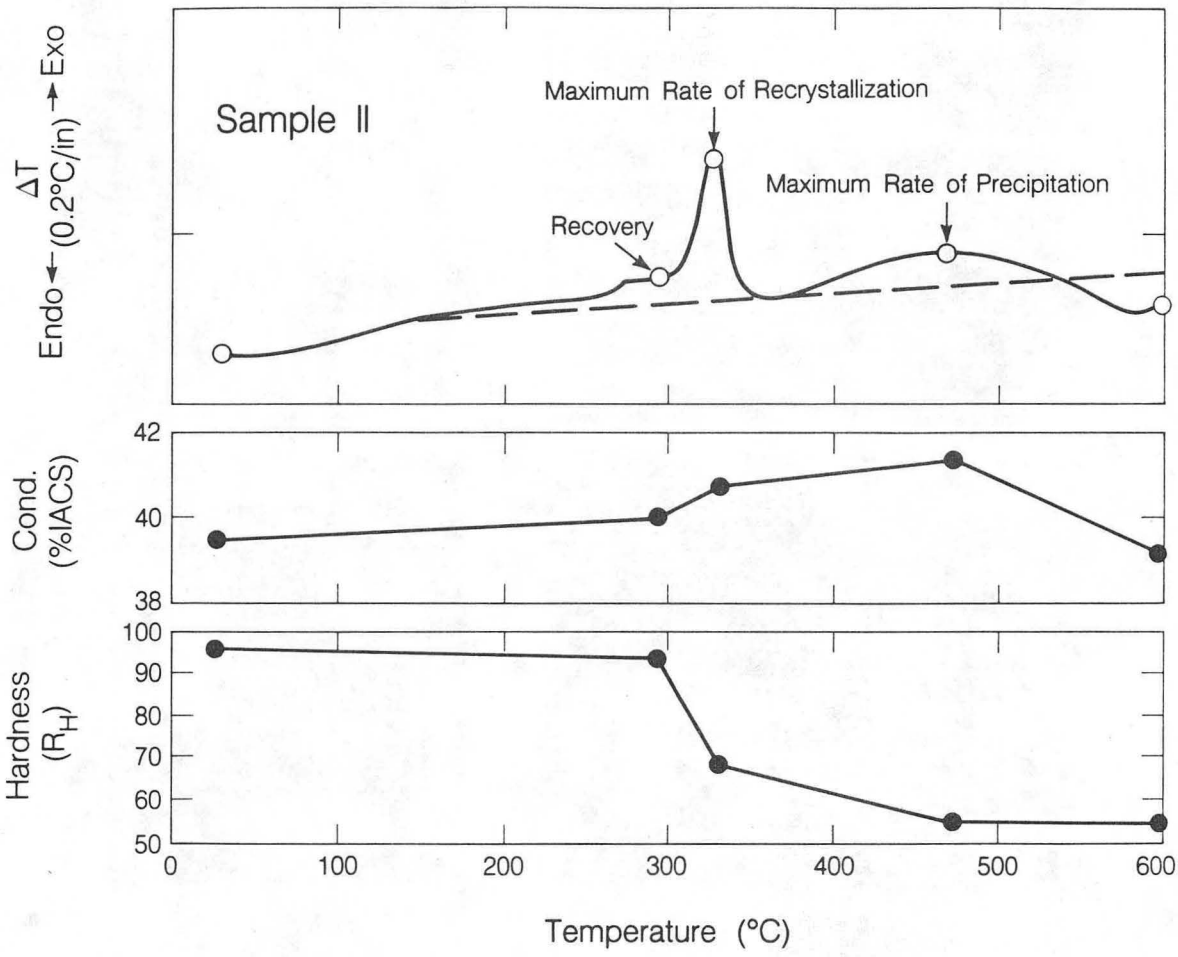
Sample II
Maximum Rate of Recrystallization
Maximum Rate of Precipitation
Recovery
ΔT
Endo ← (0.2°C/in) → Exo
Cond. (%IACS)
42
40
38
Hardness (R_H)
100
90
80
70
60
50
0
100
200
300
400
500
600
Temperature (°C)
XBL 855-11140

Fig. 5

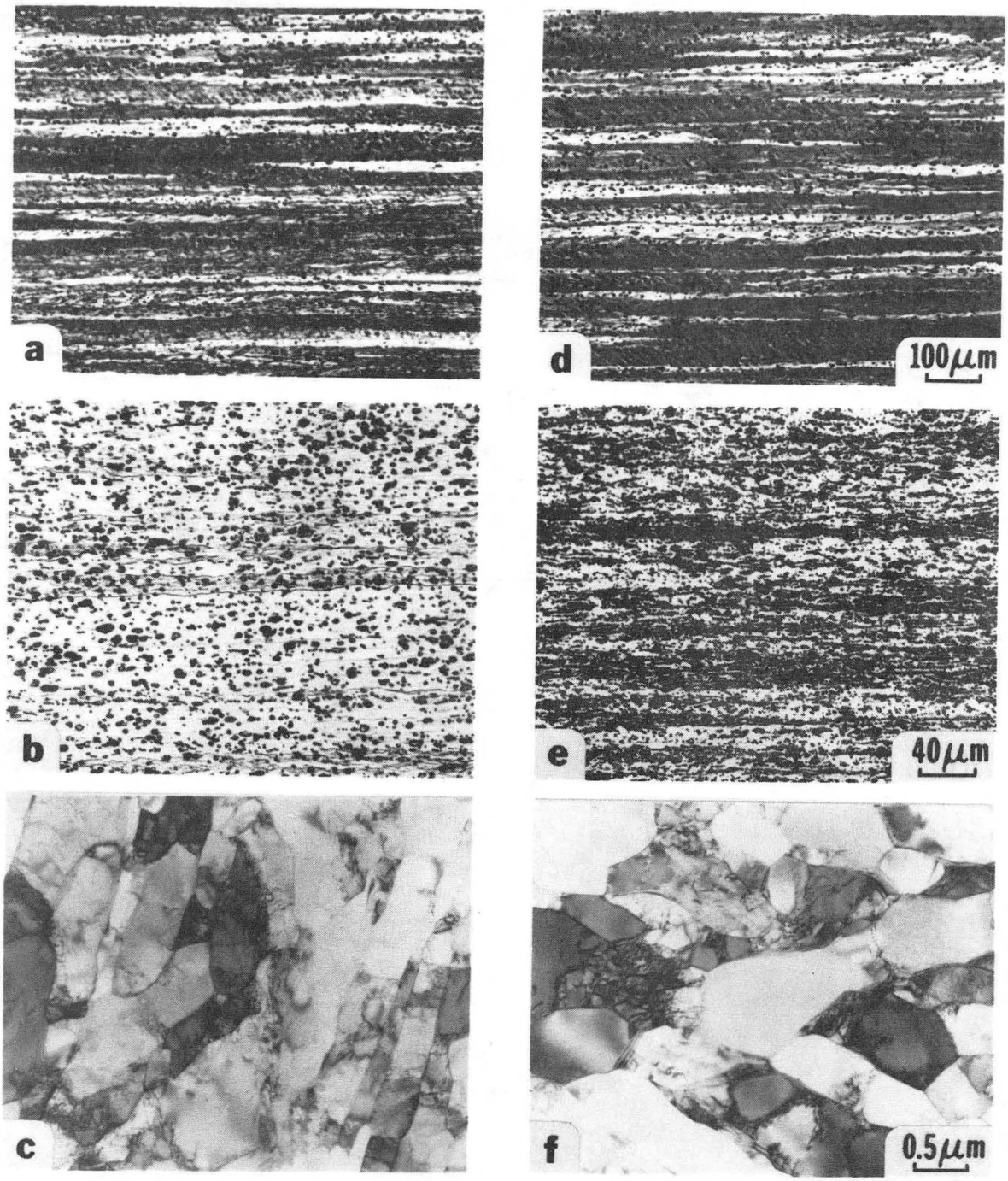

XBB 855-3948

Fig. 6

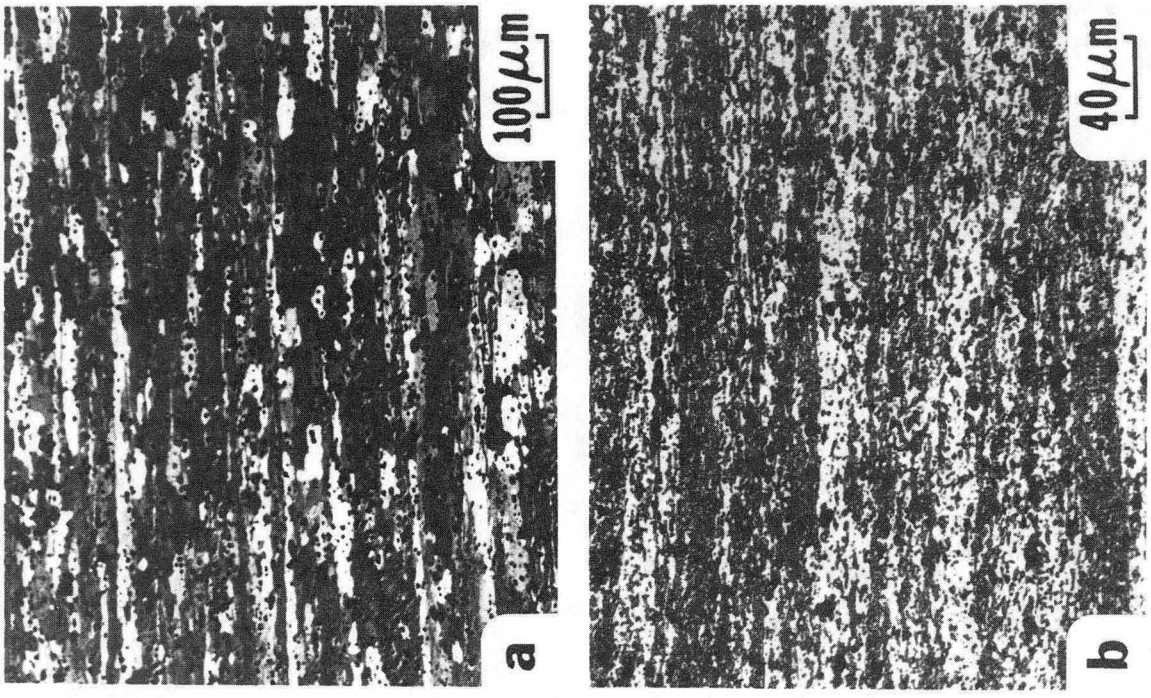

XBB 855-3949

Fig. 7

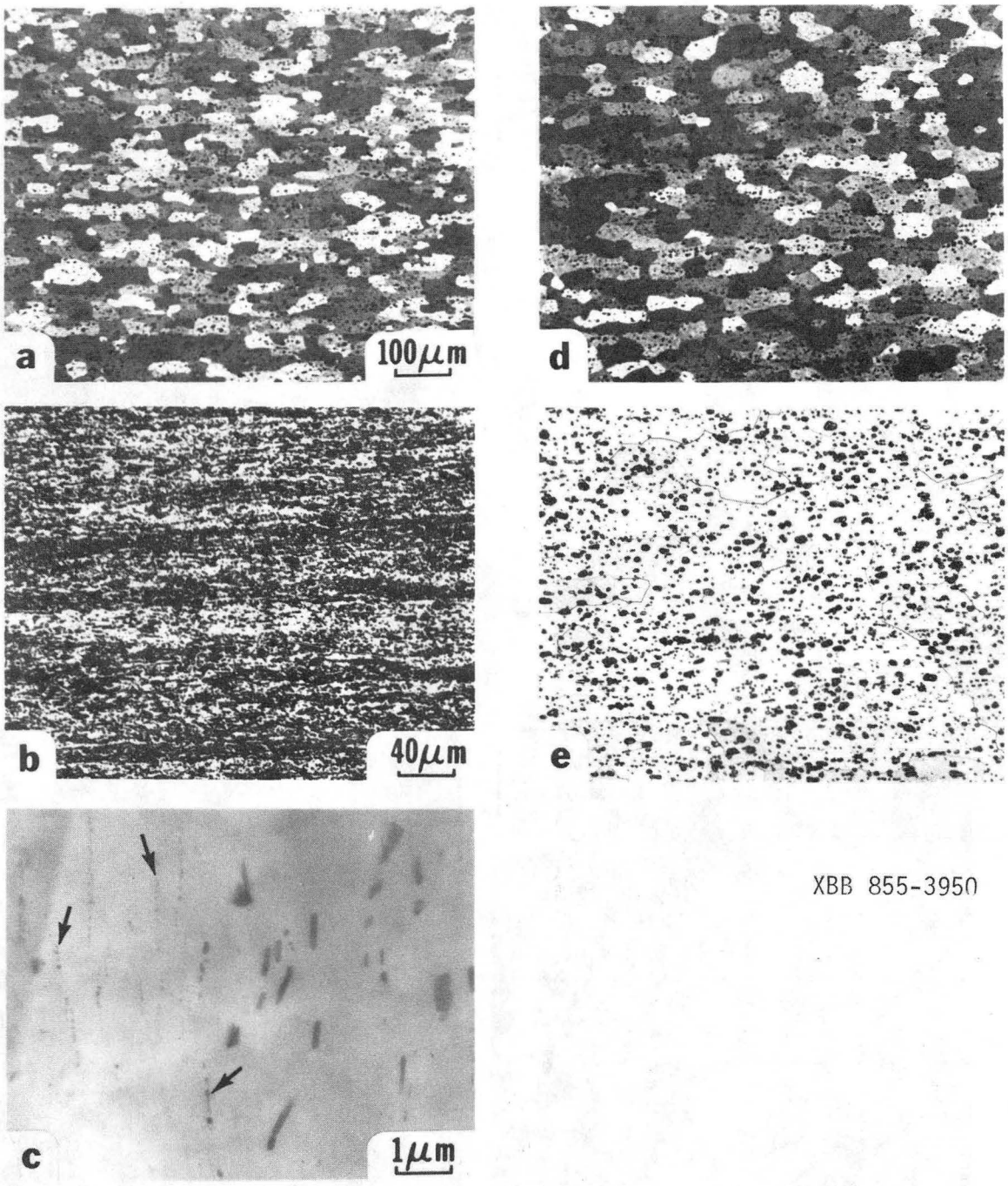

XBB 855-3950

Fig. 8

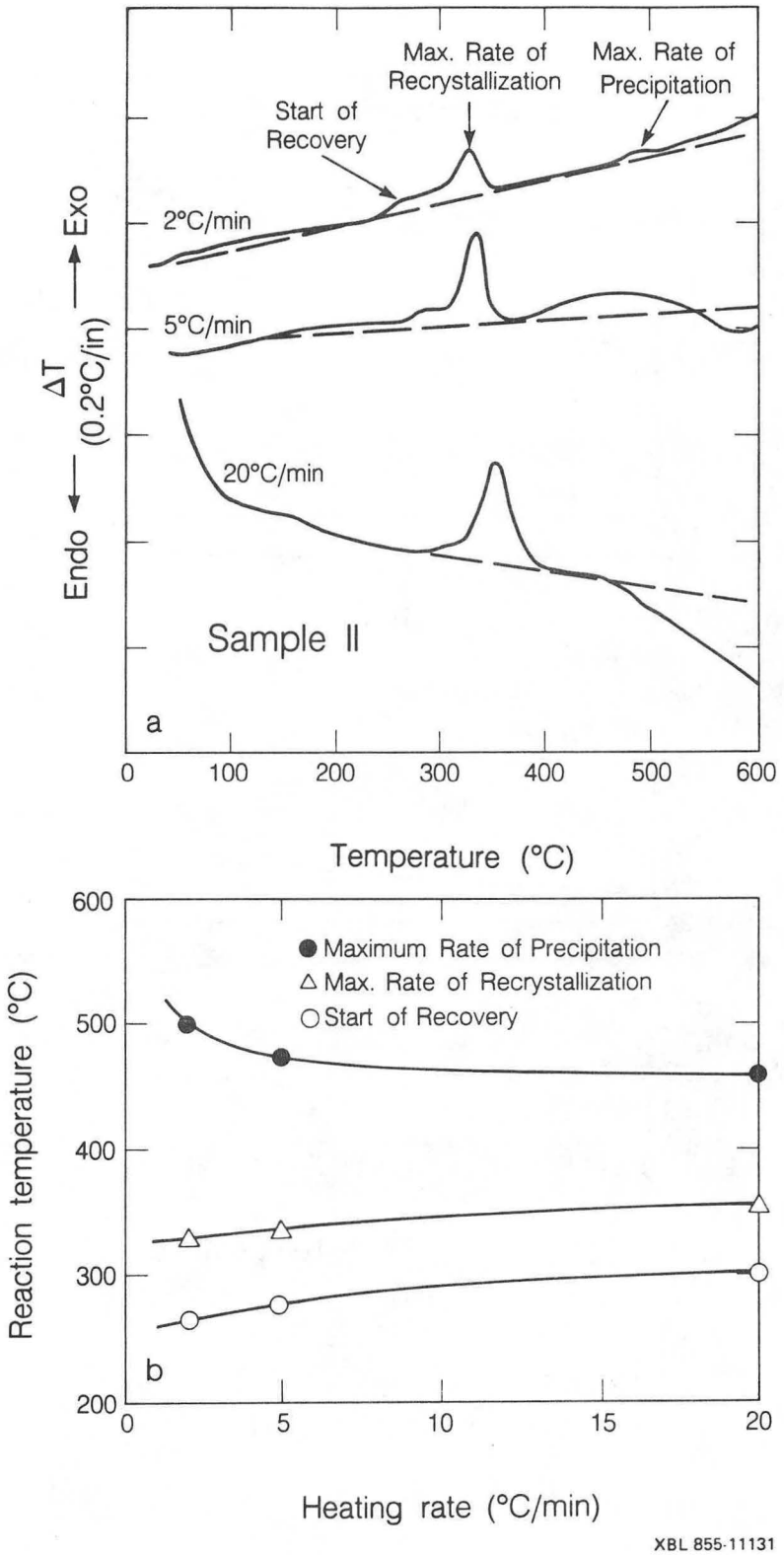
Max. Rate of Recrystallization
Max. Rate of Precipitation
Start of Recovery
2°C/min
5°C/min
20°C/min
Sample II
a
ΔT (0.2°C/in)
Endo
Exo
0
100
200
300
400
500
600
Temperature (°C)
Maximum Rate of Precipitation
Max. Rate of Recrystallization
Start of Recovery
Reaction temperature (°C)
600
500
400
300
200
b
0
5
10
15
20
Heating rate (°C/min)
XBL 855-11131

Fig. 9

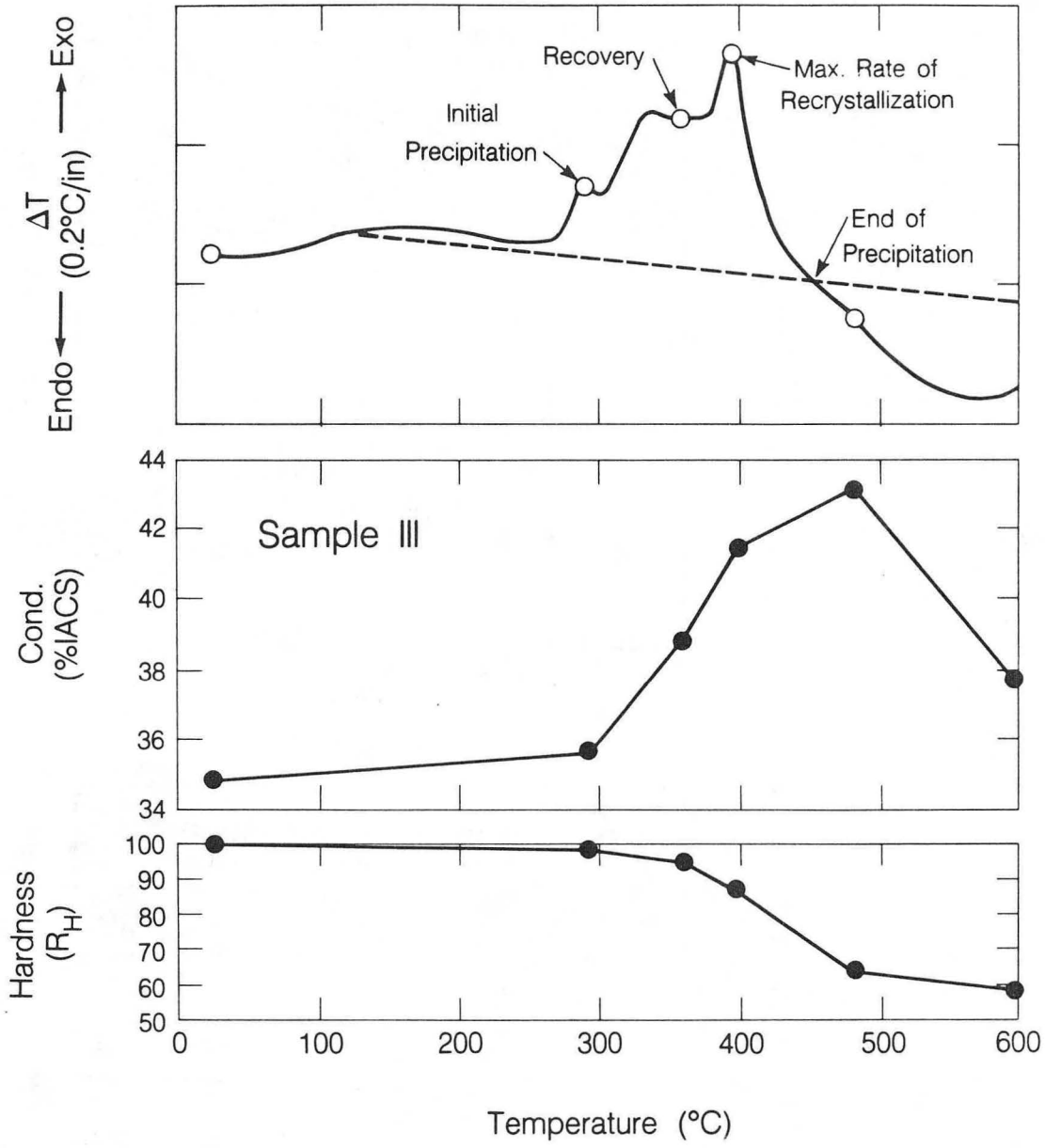
ΔT
(0.2°C/in)
Endo
Exo
Recovery
Max. Rate of
Recrystallization
Initial
Precipitation
End of
Precipitation
Sample III
Cond.
(%IACS)
Hardness
(R_H)
Temperature (°C)
XBL 855-11142

Fig. 10

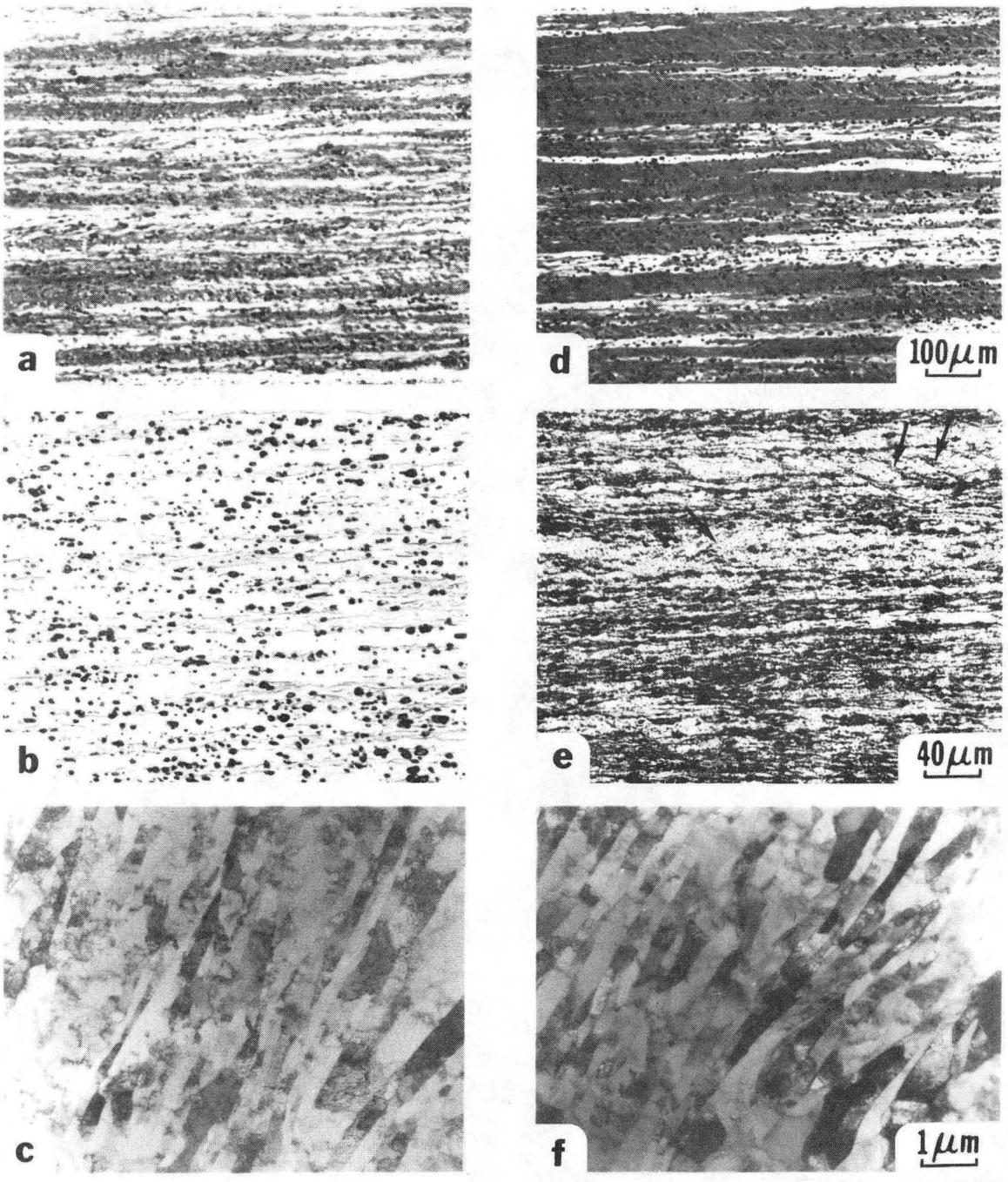

XBB 855-3951

Fig. 11

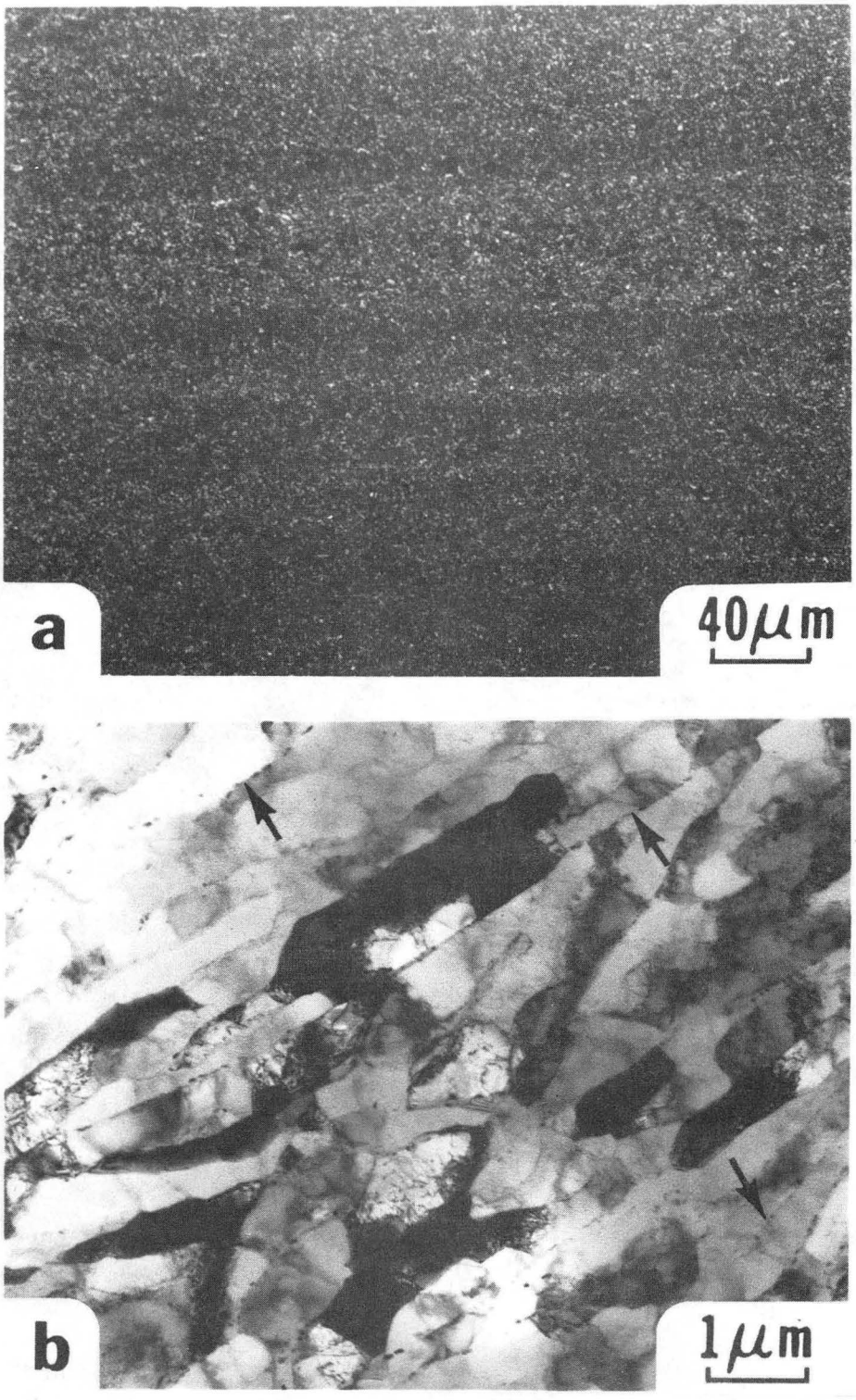

XBB 855-3957

Fig. 12

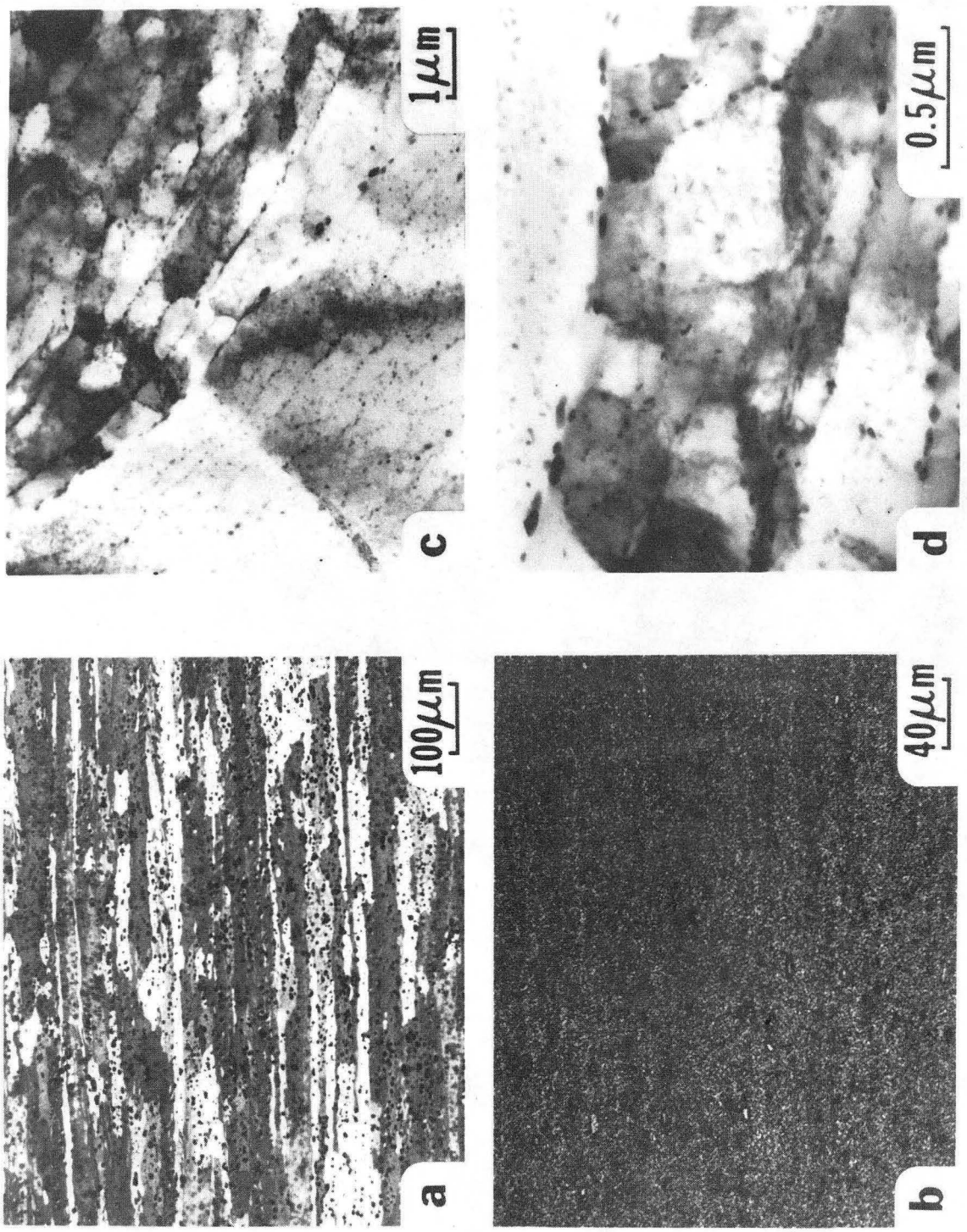

XBB 855-3952

Fig. 13

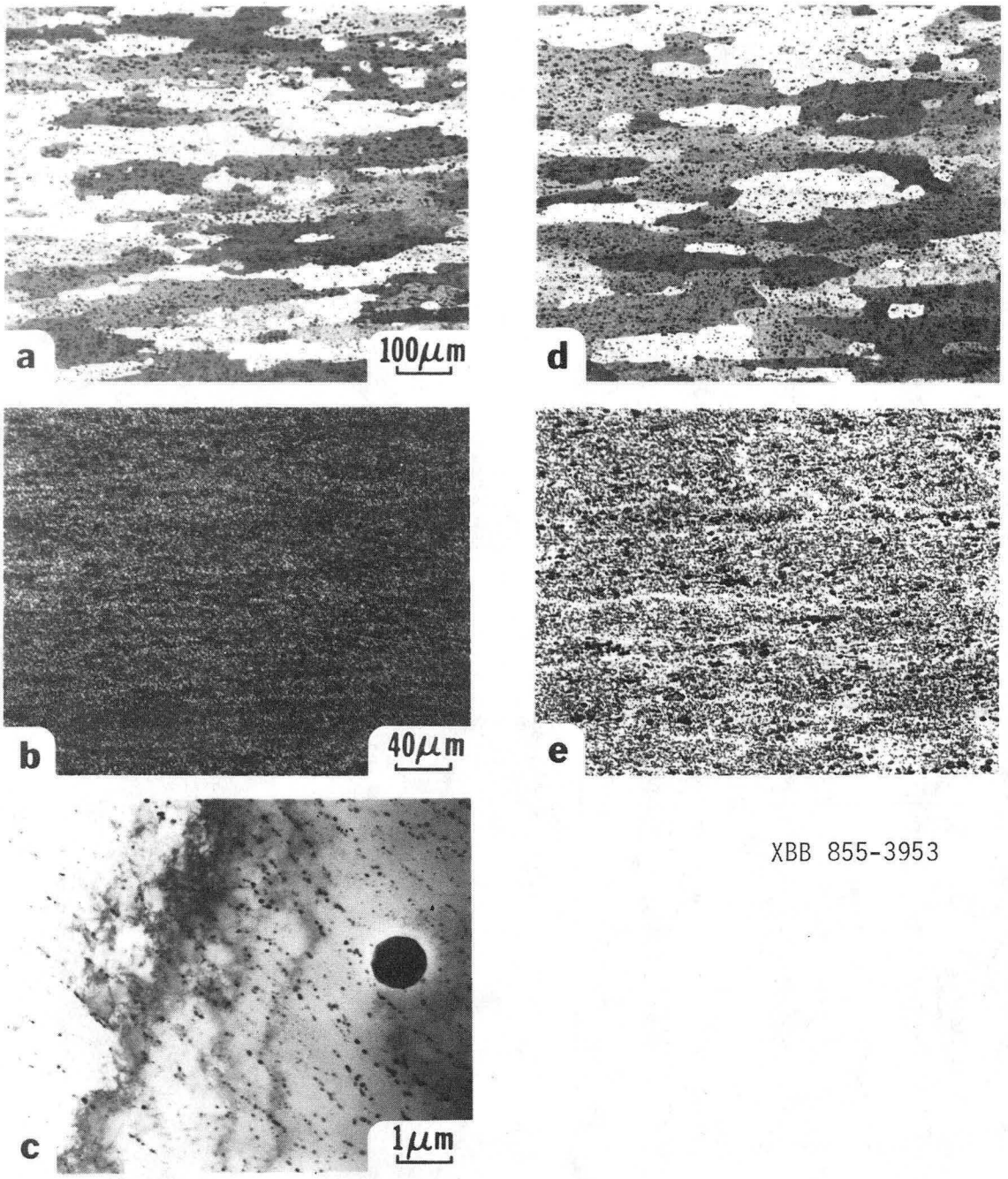

XBB 855-3953

Fig. 14

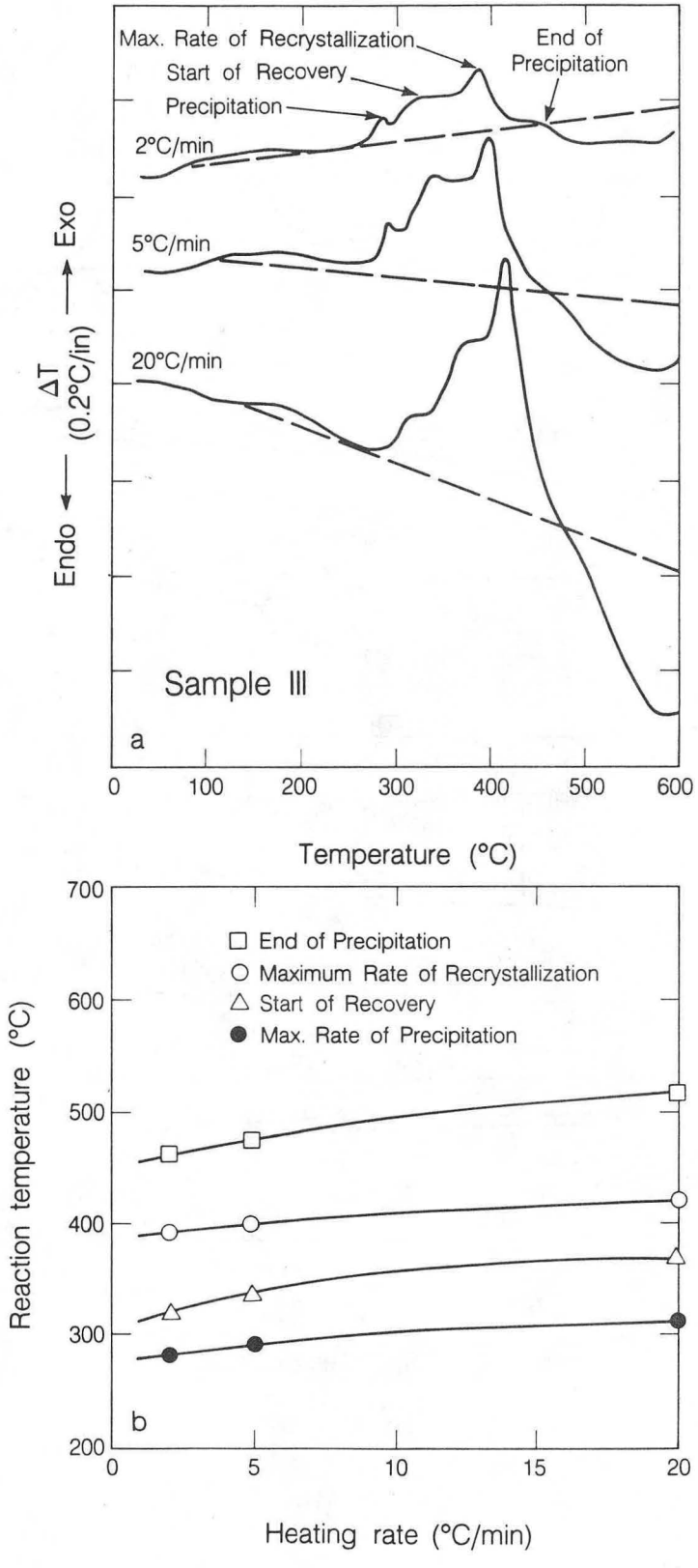
Max. Rate of Recrystallization
Start of Recovery
Precipitation
End of Precipitation
2°C/min
5°C/min
20°C/min
Endo ⟵ ΔT (0.2°C/in) ⟶ Exo
Sample III
a
0
100
200
300
400
500
600
Temperature (°C)
700
600
500
400
300
200
Reaction temperature (°C)
End of Precipitation
Maximum Rate of Recrystallization
Start of Recovery
Max. Rate of Precipitation
b
0
5
10
15
20
Heating rate (°C/min)
XBL 855-11130

Fig. 15

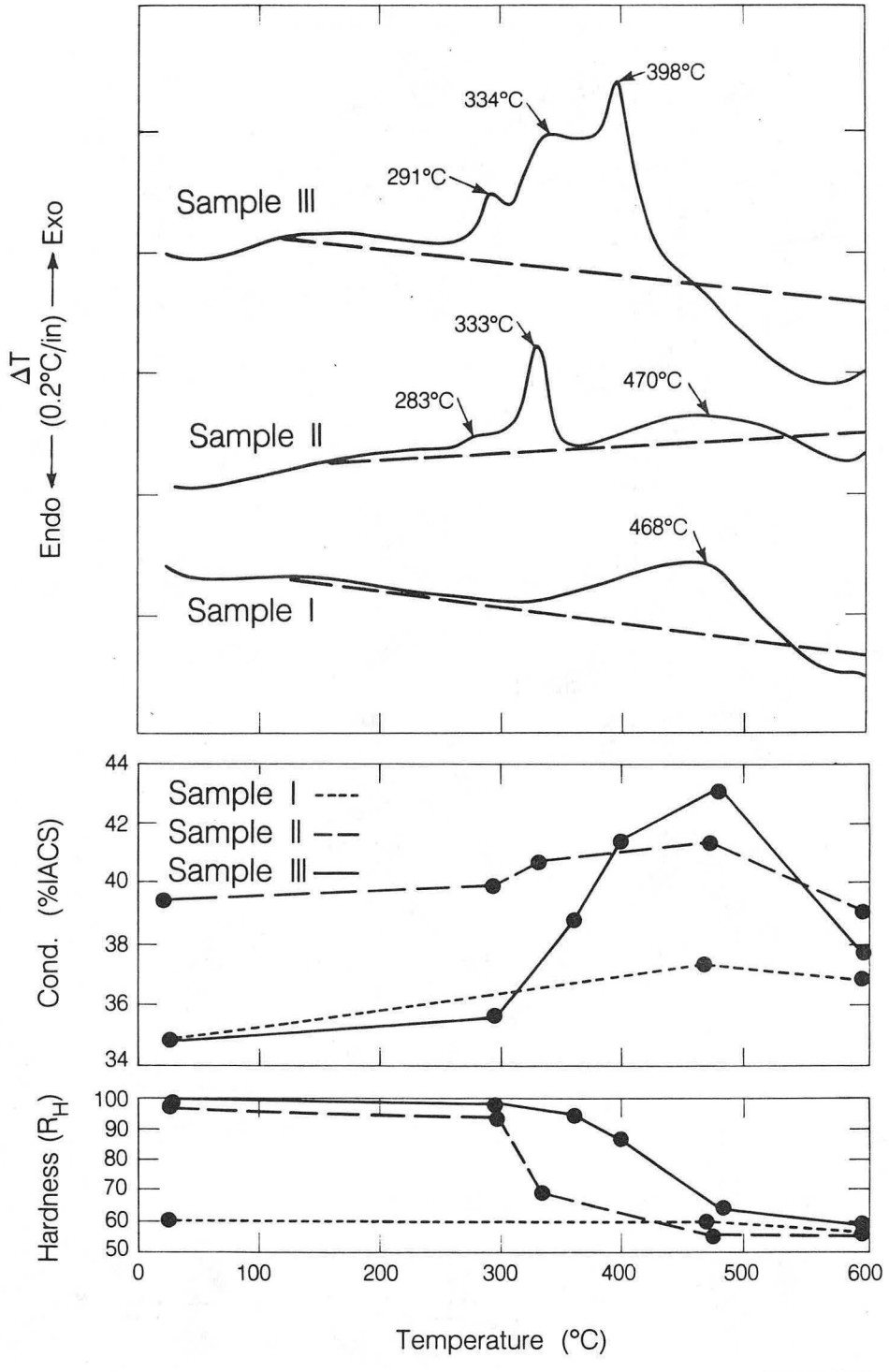
398°C
334°C
291°C
Sample III
333°C
470°C
283°C
Sample II
468°C
Sample I
ΔT
Endo ← (0.2°C/in) → Exo
Sample I ----
Sample II – –
Sample III ——
Cond. (%IACS)
Hardness (R_H)
Temperature (°C)
XBL 855-11139

Fig. 16

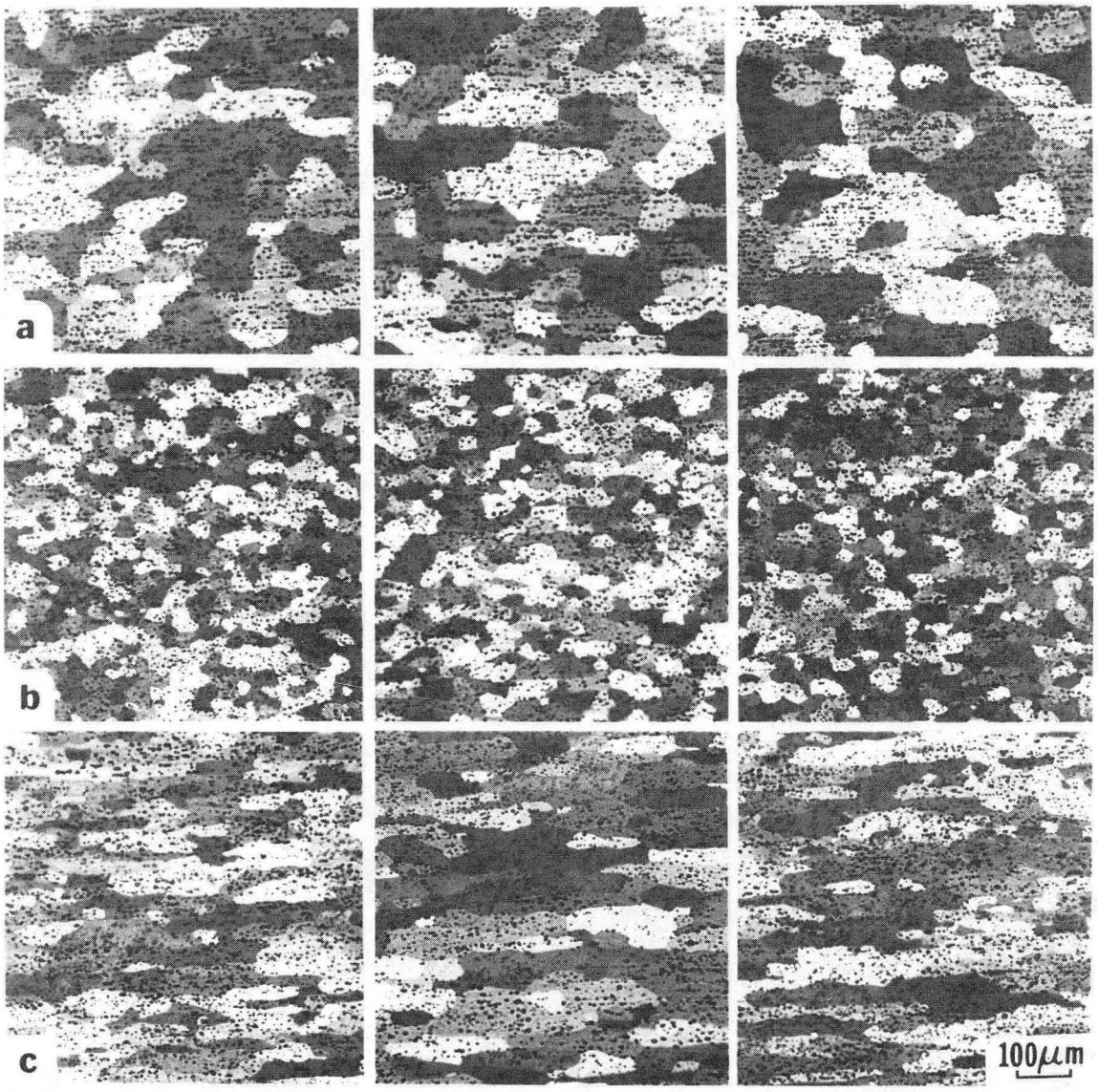

XBB 855-3955

Fig. 17

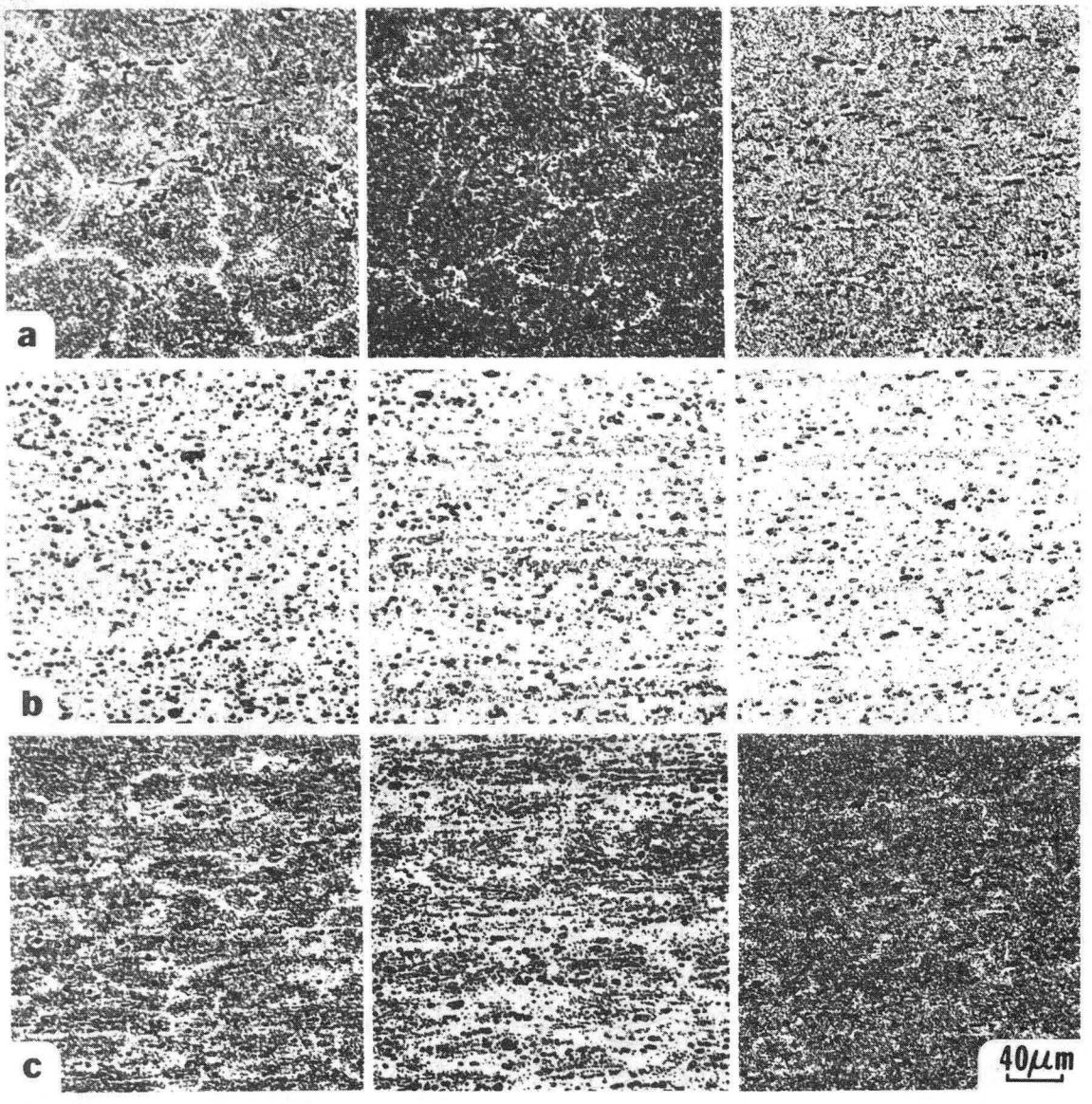

XBB 855-3956

Fig. 18

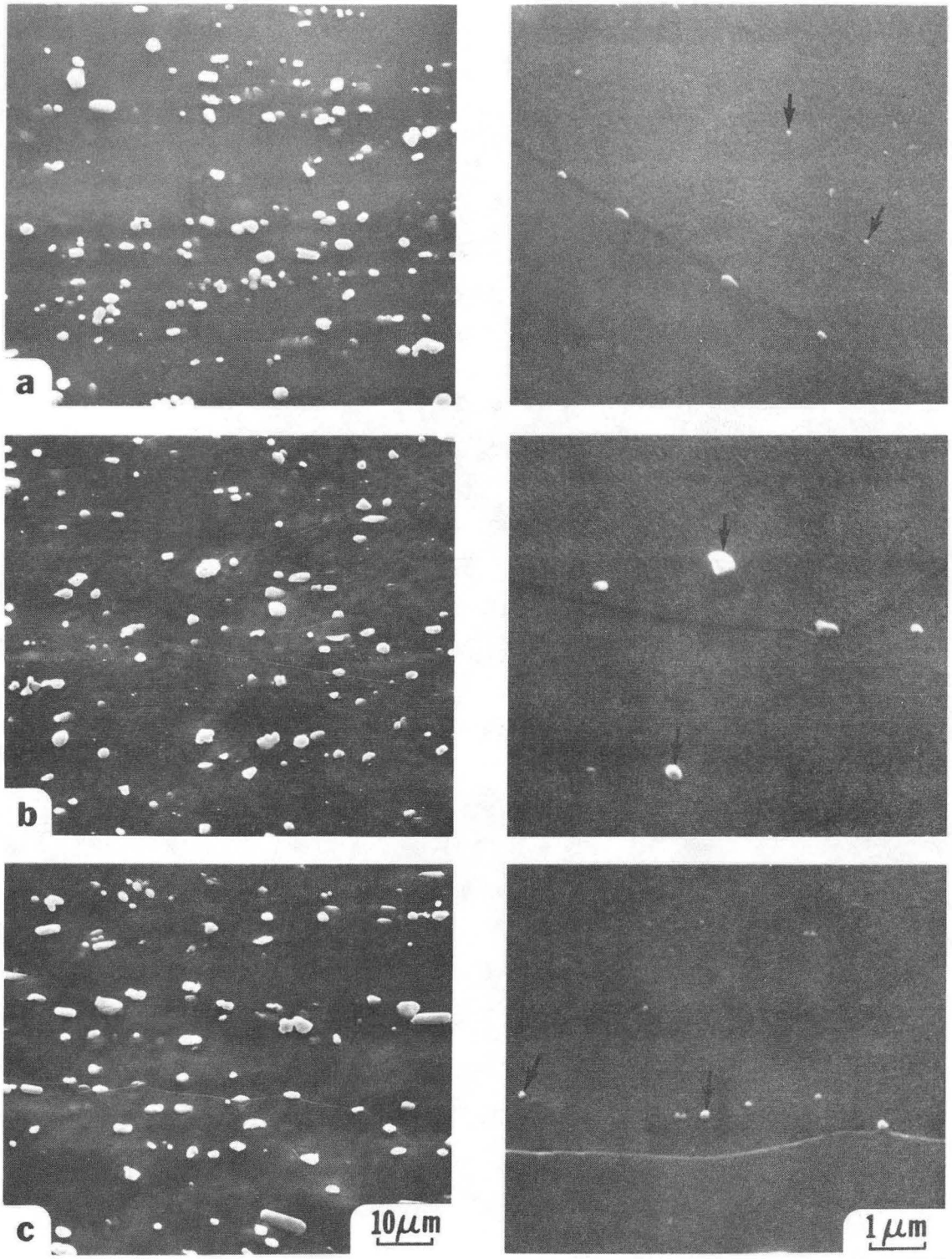

XBB 855-3954

Fig. 19

LAWRENCE BERKELEY LABORATORY
TECHNICAL INFORMATION DEPARTMENT
UNIVERSITY OF CALIFORNIA
BERKELEY, CALIFORNIA 94720